KROLL, H. (1971). *Feldspäte im System* $K[AlSi_3O_8]$–$Na[AlSi_3O_8]$–$Ca[Al_2Si_2O_8]$: Al, Si *Verteilung und Gitterparameter, Phasen-Transformationen und Chemismus.* Thesis, Westfälischen Wilhelms-Univ., Münster.
LAVES, F., CZANK, M. & SCHULZ, H. (1970). *Schweiz. miner. petrogr. Mitt.* **50**, 519–525.
LAVES, F. & GOLDSMITH, J. R. (1955). *Z. Kristallogr.* **106**, 227–235.
LOEWENSTEIN, W. (1954). *Amer. Min.* **39**, 92–96.
MEGAW, H. D., KEMPSTER, C. J. E. & RADOSLOVICH, E. W. (1962). *Acta Cryst.* **15**, 1017–1035.
MÜLLER, W. F. & WENK, H. R. (1973). *Neues Jb. Miner. Mh.* pp. 17–26.
RIBBE, P. H. & GIBBS, G. V. (1969). *Amer. Min.* **54**, 85–94.
RIBBE, P. H., MEGAW, H. D., TAYLOR, W. H., FERGUSON, R. B. & TRAILL, R. J. (1969). *Acta Cryst.* B**25**, 1503–1518.
RIBBE, P. H., STEWART, D. B. & PHILLIPS, M. W. (1970). Proc. Geol. Soc. Amer. Meeting, Milwaukee. Abstracts, p. 663.
SMITH, J. V. (1972). *J. Geol.* **80**, 505–525.
SMITH, J. V. (1974). *Feldspar Minerals.* Vol. 1. *Crystal Structure and Physical Properties.* Berlin: Springer Verlag.
STOUT, G. H. & JENSEN, L. H. (1968). *X-ray Structure Determination.* New York: Macmillan.
WAINWRIGHT, J. E. & STARKEY, J. (1971). *Z. Kristallogr.* **133**, 75–84.

Acta Cryst. (1976). B**32**, 3280

A Structure Analysis of the Compound $K_{0\cdot27}WO_{(3+y)}$

BY P. GOODMAN

Division of Chemical Physics, CSIRO, P.O. Box 160, *Clayton, Victoria, Australia* 3168

(*Received* 23 *January* 1976; *accepted* 12 *May* 1976)

The structure of the compound $K_xWO_{(3+y)}$ with $x \simeq 0{\cdot}27$ and $y = x/2$ has been studied by X-ray and electron diffraction. The structure resembles an ordered hexagonal tungsten bronze. Crystals for the structural study were prepared by vapour transport growth and annealed at high temperature. This preparation allowed two types of ordering to be distinguished, one involving the host WO_3 lattice and the other involving the K^+ structure. It was found that the value of y in the above formula can be varied over a certain range without a major structural change; the structural influence of small changes in O content has been studied.

1. Introduction

A study has been made of the crystal structure of the non-stoichiometric compounds $K_xWO_{(3+y)}$, where x is approximately 0·27 and y ranges between the limits of zero and 0·27/2. This study was carried out in three stages: crystal growth, diffraction study, and a study of oxidation. Initially conditions were found for growing crystals of uniform structure in plate and needle morphology by vapour transport. These were required for X-ray and electron diffraction and electron microscopy investigations, and allowed a semi-quantitative structure determination. Finally a study was made of the oxidation and reduction over a range of stoichiometry, within which the process appeared to be completely reversible, and to take place without loss of morphology. For this latter study both the vapour-grown crystals and the more readily available crystals produced by solid-state reaction were used.

A preliminary report (Denne & Goodman, 1973) gave the unit-cell parameters obtained from the vapour-grown crystals. However, at the time of that report the evidence of Deschanvres, Desgardin, Raveau & Thomazeau (1967) had not been noted. These authors studied the oxidation and reduction between the tungsten bronze and the tungstate of similar potassium content to our preparations. After a comparison of the two sets of data (*i.e.* 1967 and 1973) it became evident that our crystals were in a higher state of oxidation than originally stated. It was also evident that the earlier authors were working with twinned crystals and without the aid of electron diffraction, and consequently failed to find the true unit cell and symmetry of the structure. The twinning morphology and identification of the true symmetry was discussed in our 1973 report. It is now possible to give many additional features of the structure as a consequence of electron diffraction and electron microscope analysis, and additional chemical evidence of the type presented by Deschanvres *et al.*

2. An outline of the structure

The ordered structure consists of the addition of two almost totally independent structures, namely the WO_3 lattice which adopts a slightly distorted version of the hexagonal tungsten-bronze structure (Magnéli & Blomberg, 1951), plus a structure of K^+ ions exhibiting long and short-range ordering. After high-temperature annealing in air, long-range ordering of the K^+ ions in the **a*** direction is complete, every fourth interstitial plane being almost completely vacant. K^+ ion sites

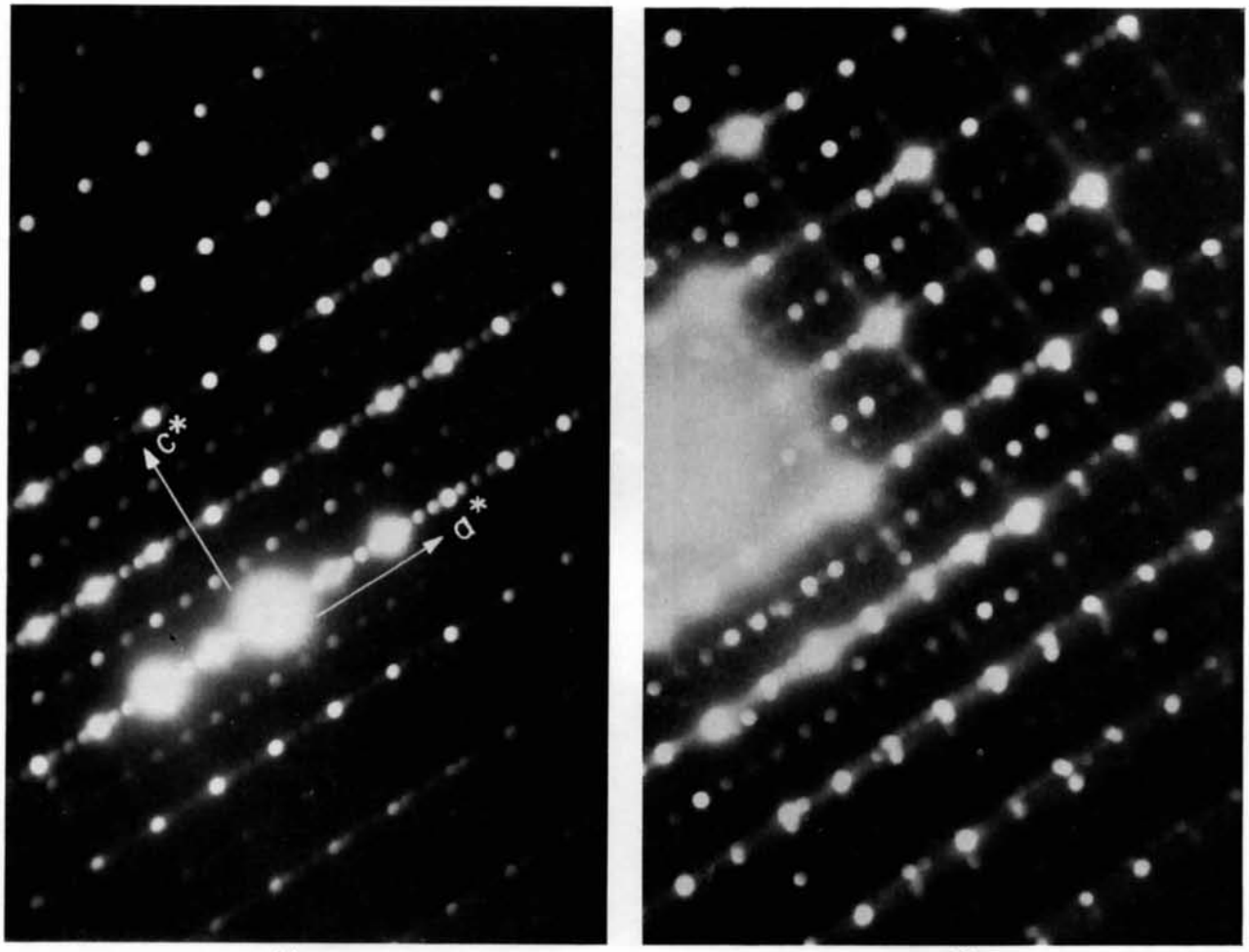

(*a*) (*b*)

Fig. 1. Selected-area diffraction patterns taken near the [010] zone axis. (*a*) Zone-axis setting. (*b*) Rotation from the zone about **c***. Arrows indicating **a***,**c*** directions are displaced slightly from the diffraction rows to avoid obscuring them.

[*To face p.* 3280

are in the tunnels approximately midway between the dense hexagonal planes of W atoms. Additional O appears to be taken up reversibly and continuously over a certain non-stoichiometric range by accommodating O^- ions along the tunnels between the K^+ sites, and possibly coplanar with the W sites, without any detectable K–O–K bonding.

Evidence for locating the additional O^- ions in tunnel sites comes from the X-ray diffraction measurements, although the scattering power of O is relatively weak; further evidence, for the z coordinates of the K^+ ions and hence of the O^- ions, comes indirectly from the diffuse electron diffraction patterns. There is, however, a need for further data to determine the z coordinates of the tunnel sites, which could only be obtained by a thorough X-ray diffraction study. The tunnel-ion z coordinates suggested in this section were initially an informed guess, based on evidence of a continuous oxidation range described in §5, within which the sublattice remains dimensionally stable, and on knowledge of the initial K_xWO_3 Magnéli structure. These coordinates, however, are not crucial to the conclusions of the present analysis.

3. Crystal growth by vapour transport

Crystals were grown on an alumina substrate at the top end of a muffle furnace with a central temperature of approximately 1350 °C. A partly covered Pt crucible containing WO_3 powder was placed at the base of the furnace. The inner sleeve of the furnace was composed of high-grade sintered alumina which, as supplied, contained a proportion of K and Na silicate complexes and no other significant impurities. WO_3 vapour was therefore transported in an atmosphere containing both Na^+ and K^+ ions. The results show that the structure will not retain Na^+ ions above 1300 °C, but that within the temperature range 1300–1350 °C the K^+ ions are retained and move relatively freely through the lattice. As a result, by maintaining a stable temperature for 24 to 36 h crystals are obtained which are Na free and have K^+ ions in ordered sites.

Spectroscopic analysis was made of the alumina substrate and also of the product. This yielded information beyond the sensitivity of microprobe analysis and allowed us to rule out any significant heavy-metal impurities. Microprobe analysis of the crystals then allowed us to rule out Al or Na as impurities, and to determine x in $K_xWO_{(3+y)}$ as $0{\cdot}27 \pm 0{\cdot}02$ by comparison with a standard preparation.

Under optical microscopy the crystal plates appeared perfect, showing constant interference colours over large regions and having sharp crystallographic edges. Thick crystals were yellow and transparent. Hexagonal needle crystals which were also formed, and which proved to be composed of hexagonally twinned plates (Denne & Goodman, 1973), were also yellow, with only occasional black tips. Occasionally platelets occurred of only a few hundred ångström thickness and hence directly accessible to transmission electron study. An advantage of this preparation was that crystals suitable for electron diffraction, and with a contant structure over several microns area, could be selected by optical microscopy. The ordered regions were therefore extensive, and no mechanical grinding, which can affect the structure, was necessary.

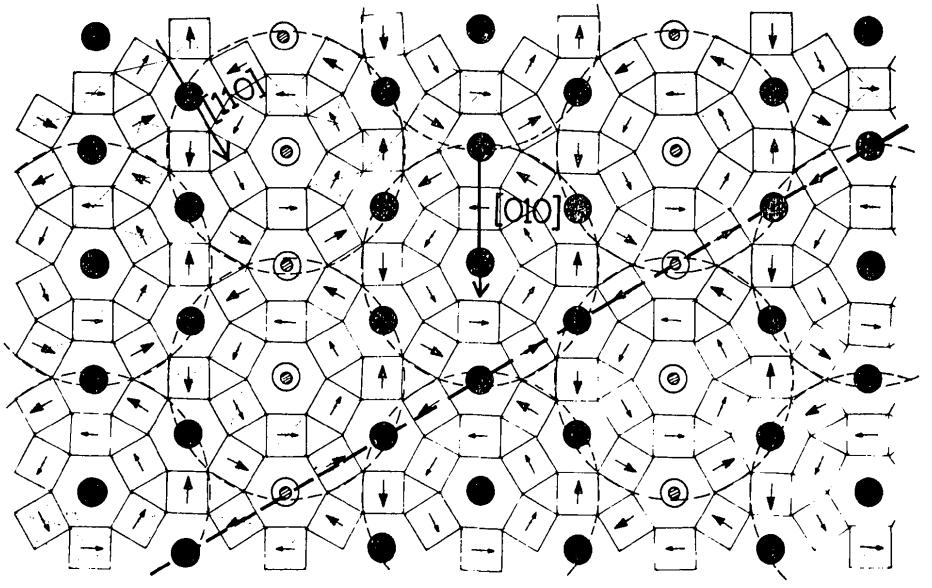

Fig. 2. Schematic [001] projection of the structure for one atomic layer (half a unit cell) in which the WO_3 host lattice is shown as linked octahedra by means of lines only, and K^+ ions are shown as filled circles for full occupation, and semi-shaded circles for fractional occupation. Small arrows represent directions of W atom shifts consistent with a second, $2a \times 2b$, superlattice. The broken diagonal line indicates the observed plane of easy cleavage.

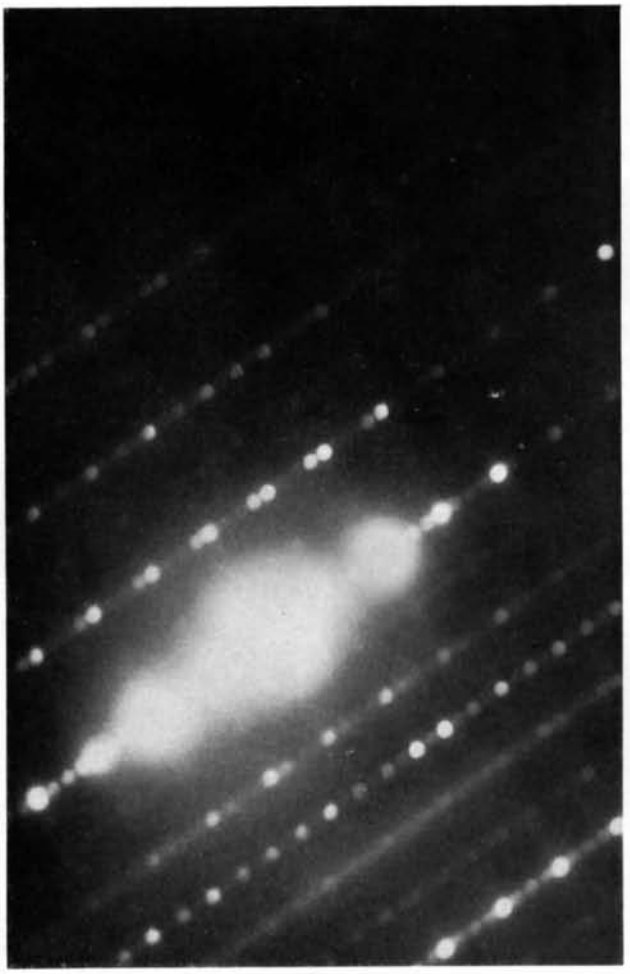

(*c*)

Fig. 1 (*cont.*). (*c*) Rotation from the zone about **a***.

To face p. 3281

4. Diffraction evidence from the vapour-grown preparation

Platelets used for electron diffraction grew with {110} surfaces, and the needles used for X-ray diffraction consisted of these plates twinned hexagonally around the *c* axis. Because of this morphology, X-ray Weissenberg patterns could be used to determine the sublattice structure, and the twinning allowed a small departure of the subcell from hexagonality to be measured (Denne & Goodman, 1973).

Selected-area, single-crystal patterns were taken by electron diffraction near the [010] and [110] zone axes. The [010] zone selected-area pattern is shown in Fig. 1(*a*). Along lines $l=2n$, we find a fourfold superstructure reflexion set. The fourth order is a W reflexion expected from the projected structure (see Fig. 2), and the eighth order represents the basic (tilted) octahedral dimension. A second superstructure appears along lines $l=2n+1$, where the 6·5 Å spacing is doubled. When a small rotation is made about **c*** away from the zone setting (Fig. 1*b*) the twofold ($l=2n+1$) superlattice remains sharp while the fourfold ($l=2n$) superlattice deteriorates into diffuse streaks. Upon rotation from the zone about **a***, however, the fourfold superlattice reflexions remain sharp (Fig. 1*c*). Hence we can associate the twofold structure with the three-dimensional ordering, and the fourfold structure with planar ordering, since all projections containing the [*h*00]* vector give sharp fourfold reflexions. The diffuse streaks which occur with the [*h*00]* vector out of the plane of the projection indicate disorder within the set of (*h*00) planes. The set of Fig. 1 gives us the dimensions of a monoclinic unit cell ($a=29·2$, $b=14·6$, $c=7·6$ Å) with $\gamma\simeq 120°$. The electron diffraction evidence and a knowledge of the chemical composition are sufficient to show that the three-dimensional sharp superlattice is an ordering in the host WO_3 lattice, and that the planar ordering is an ordering of vacancies along the interstitial sites partially occupied by K^+ ions. The vacancy planes causing the fourfold superlattice will actually have a small K^+ population due to the excess of x over 0·25 in the K_xWO_{3+y} formula.

The two superlattices are further distinguished by their different relative scattering powers. In electron diffraction the weights of the reflexions from the two superlattices are roughly comparable in intensity, whereas in X-ray diffraction the WO_3 superlattice reflexion is barely half the strength of that from the K^+ superlattice. This difference is possibly due to the WO_3 superlattice being formed by a set of small displacements of W nuclei from ideal positions, which produces a relatively large electrostatic field. A rotational shear mechanism (Bursill & Hyde, 1972) was the only model considered which could explain the unit-cell size, and also the alternating nature of the intensities along the **a*** direction of the $k=2n+1$ layer lines. This mechanism must exist as a strain created by a few degrees rotation and not a complete shear as in the $K_2W_4O_{13}$ structure (which would give completely unacceptable structure factors), as indicated in Fig. 2. Detailed refinement of this superlattice was not attempted. One requirement, which could be met by this model, is for parallel displacement vectors along the line indicated of the plane of easy cleavage of the structure. By contrast with the tungsten-bronze structure where easy cleavage is perpendicular to the *c* axis, this structure apparently has a component of displacement parallel to the *c* axis.

The [110] orientation, selected-area patterns show the characteristic pattern of Fig. 3. In this projection, provided that the structure in Fig. 2 is correct in outline, we expect to find *hh*0 reflexions of appreciable strength only for $h=4n$, and this agrees with observation. The $l=2n$ superstructure reflexions have completely degenerated into streaks, and another set of streaks passes perpendicular through the *hh*0 spots for which $h=4n$. These sets correspond to $3·8\times 3·6$ Å short-range ordering, which, on the assumption that this scattering arises from a finite K^+ population in the 'vacancy' planes, indicates: (*a*) the formation of finite K^+ strings along the hexagonal tunnels, and (*b*) K^+ ordering between tunnels. These two directions of ordering may be associated with two separate processes occurring with oxidation, as described below. Interaction of streaks with sharp reflexions along the lines $l=2n$ shows a centred geometry; if we now re-index the pattern for convenience on the basis of the projected subcell with $a=7·3$ Å, spots of index $h=2n$ are reduced and those of index $h=2n+1$ are increased in intensity. This can be best seen in Fig. 3 along the lines $l=\pm 2$ when neighbouring reflexions of approximately the same strength are compared. Thus in the spots marked with arrows *A* and *B* in this figure, spots *A* ($h=2n+1$) have a lateral broadening where they inter-

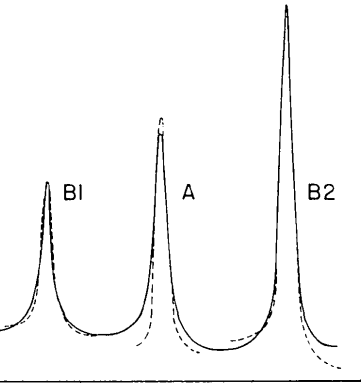

Fig. 4. Microphotometer traces taken across three spots identified as *B*1, *A*, and *B*2 along the line $l=2$ in Fig. 3. Full lines represent the lateral scan and broken lines represent individual vertical scans across the same spots. Note the comparative lateral broadening of the *A* peak (difference between full and broken lines). Note also that the third peak, though appreciably higher, is not broader than the second peak. Actual ratios of basal peak breadth to peak height, for *B*1, *A*, and *B*2, are 25/70, 40/90, and 37/160 respectively.

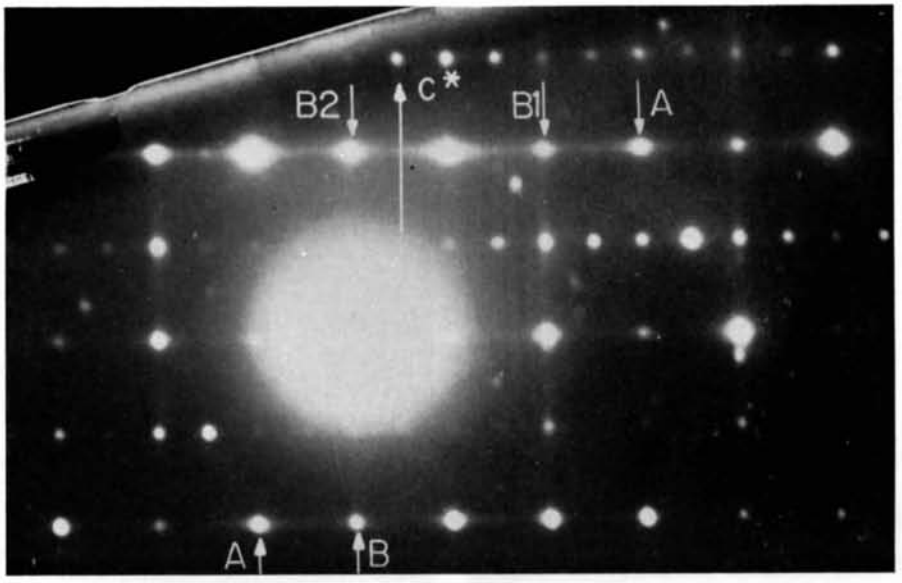

Fig. 3. Selected-area pattern obtained from [110] zone axis. The centred geometry caused by interaction of disorder streaks cutting the pattern on a 3·8 × 3·6 Å unit is best seen by comparing the diffuse streak around type *A* spots with those around type *B* spots.

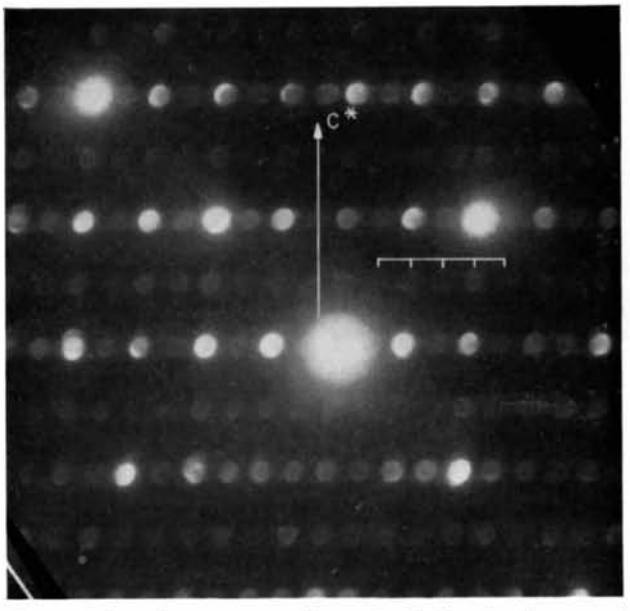

Fig. 5. Selected-area pattern from the [010] axis of a crystal which has been reduced by heating for several hours *in vacuo* at 600–700 °C, after original annealing in air. Only the twofold superlattice is observed, with a spacing of 13 Å, and this spacing is indicated by a ruler. Note: the lack of orthogonality in this pattern is due to a slight mis-setting from the zone axis, combined with the sloping crystal shape transform arising from the fact that the normal to the crystal surface is at 30° to the zone axis [compare with the non-orthogonality in Fig. 1(*c*)].

[*To face p.* 3282

act with the streaks, while those marked *B* have a laterally compressed intensity distribution. This effect can be demonstrated from the microphotometer traces from spots of comparable intensity. Fig. 4 shows the traces from three spots marked in Fig. 3. The traces were taken by lateral scan (scan direction along the streak) and vertical scan (scan direction perpendicular to the streak), both cases with a slit perpendicular to the scan direction. Typically, lateral broadening of the *A* spots shows from (*a*) the ratio of the lateral-to-vertical spot dimension, and (*b*) the ratio of breadth-to-height of *A* peaks as compared to *B* peaks (see Fig. 4 caption). Given that the K^+ ions are in the projected tunnel site positions shown in the projection of Fig. 2, then this centred geometry indicates that the ion sites are approximately midway between the W planes in the **c** direction.

The complete absence of streaks through the $l=2n+1$ lines corresponding to 7·6 Å is evidence against the formation of K–O–K molecular units along the finite strings, and confirms that the occupation probability of a site is uninfluenced by the twofold ordering of the host structure in the **c** direction.

5. Oxidation and reduction

If we start with the fully reduced tungsten-bronze structure prepared in the normal way by solid-state reaction, this may be oxidized in stages according to Table 1.

Oxidation and reduction can be performed by heating to between 600 and 700 °C in air and vacuum respectively. This occurs without loss of external crystal faces. After an initial and relatively small oxidation there is a fundamental change in the appearance and hardness of the compound, indicated in the table, which is not easily reversed. As determined from the diffraction pattern, the border in the table represents the adoption of the $2a\times 2b$ rotational superlattice. At the same time an ordering of K^+ sites commences together with a partial fourfold ordering of vacancies. This ordering is complete at the high-oxygen end of the range, and, provided there is adequate annealing, is coherent over large regions.

The K^+ ordering can be described in two stages, according to the present interpretation of the evidence. At first there is a tendency towards linear ordering along the hexagonal tunnels. Thus strings of K^+ ions are formed which lead to completely occupied, and almost completely empty, tunnels. Next there is interaction such that empty tunnels tend to aggregate into planes. This interaction between tunnels can be supposed to depend upon the modification of the structure leading to the $2a\times 2b$ basic superlattice, in which there is some electronic communication between neighbouring pairs of tunnels.

The mobility of the K^+ ions and vibrational amplitudes of the host lattice are increased by temperature, so that high-temperature annealing has an appreciable effect in producing large single domains. The reduction, by heating above 600 °C in vacuum, stops at the vertical line in Table 1. If this is carried out with crystals grown at a high temperature, the $2a\times 2b$ superlattice remains and gives sharp diffraction spots (see Fig. 5), although the fourfold superlattice is completely removed. If non-annealed crystals are used as starting material, streaks replace these sharp spots. However, electron microscope observations suggest that this is likely to result from the limited size of ordering domains rather than lack of long-range order (Goodman & McLean, 1976).

This result of reduction demonstrates that the basic WO_3 superlattice is independent of the vacancy ordering of the K^+ sites (but the reverse is probably not true). Another demonstration of this fact, and of the rigidity of the WO_3 framework, is obtained by preferential mechanical shearing. When the original platelets are held between two glass slides and sheared by sliding one surface across the other, the crystals are sprung into thin layers parallel to [110]. These sheared crystals show only the $2a\times 2b$ superlattice under electron diffraction examination (see Fig. 6), the planar ordering of vacancies having been destroyed by the mechanical strain.

Table 1. *Observed behaviour of the tungsten bronze* $K_{0\cdot 27}WO_{(3+y)}$ *under oxidation and reduction, showing the limits of the stoichiometric range which may be covered by heating the specimen to a temperature between* 600–700 °C, *in air and in vacuo respectively*

	Fully-reduced tungsten bronze	Reversible range Oxidation ⇄ Reduction			
Optical characteristics of macrocrystals	Black in reflected light	Black in reflected light	Dark green in reflected light	Light green in reflected light	Yellow in reflected light
	Opaque in thin sections	Translucent in thin sections			
Properties on grinding	Crystals hard. Fine powder is black	Crystals soft. Fine powder is pale yellow in reflexion			

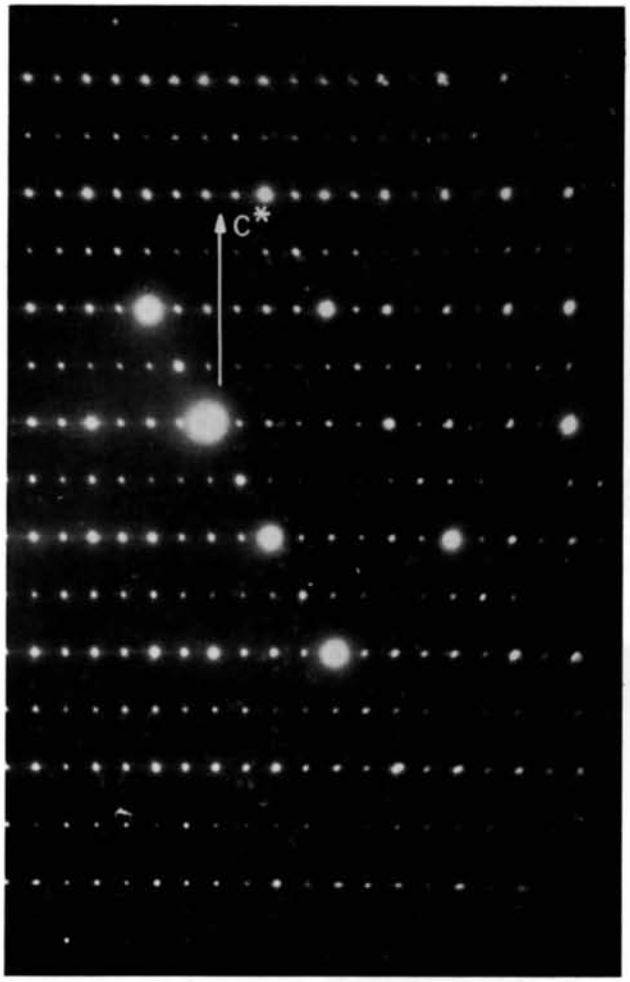

Fig. 6. Selected-area pattern from a crystal which has been fully oxidized and annealed, and then subjected to preferential mechanical shear. In this case, in spite of a large misetting of the crystal, all diffraction spots on the $2a \times 2c$ net are visible, indicating extensive layering perpendicular to the crystal surface.

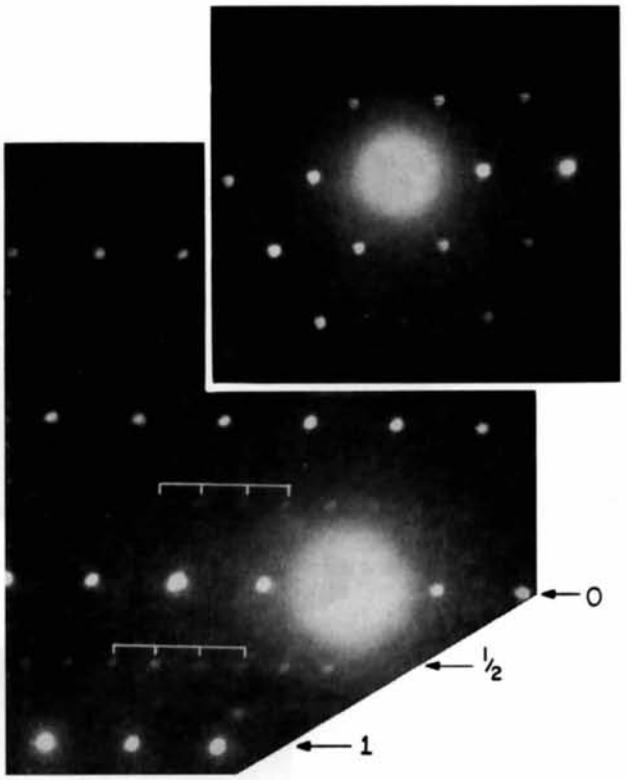

Fig. 7. Two selected-area diffraction patterns from a black tungsten-bronze specimen. (*a*) Hexagonal [001] setting. (*b*) Rotation from [001] setting showing weak extra spacings in upper-layer lines, which are indicated by rulers. The values given for l, of $0, \frac{1}{2}, 1$, are for a 3·8 Å c spacing.

[*To face p.* 3283

6. Estimation of structure factors

X-ray and electron diffraction structure factors for the $h00$ reflexions were calculated for the ordered K^+ vacancies leading to the fourfold superlattice. Table 2(*a*) shows these structure factors for different O compositions, namely with and without additional tunnel O atoms, corresponding to $y=x/2$ and $y=0$, respectively, in the formula K_xWO_{3+y}. Table 2(*b*) shows electron-diffraction structure factors calculated with $y=x/2$, but for three different electron distributions or ionicities as described below. Use is made here of the fact that the X-ray structure factors are insensitive to the ionicity, and the electron factors insensitive to the O content. No account was taken of the second superlattice caused by small lattice distortions since to do this would have been very difficult at this stage; for this reason reflexion ratios which are relatively uninfluenced by this omission were chosen for comparison with experiment. Furthermore the $h00$ reflexions are independent of the z coordinates of tunnel ions. In Table 3(*a*) the ratio F_{800}/F_{700} is tabulated for X-rays, kinematic scattering* being assumed. The experimental measurement was made from Weissenberg film records and was necessarily of limited accuracy but should be sufficiently good to distinguish between the two models for which calculated structure-factor ratios appear in Table 3(*a*). Agreement is satisfactory only for the fully oxidized model, $y=x/2$, in which the additional O ions or atoms are located in tunnel sites. In Table 3(*b*) the I_{400}/I_{100} ratio is tabulated for electron diffraction, assuming only ($h00$) systematic interactions and choosing patterns for this condition. The inaccuracy of the crystal thickness measurement (from a scanning electron microscope survey) as well as the use of the systematic interaction approximation limits use of the table to ruling out some of the more extreme models. Obviously much more could be learnt from accurate convergent-beam data, but such data were difficult to obtain with the apparatus available because of the high volatility of the compound.

As shown in Table 3(*b*), model 1, with K^+ ions (and O^- ions) in the tunnel sites and excess donated negative charge unlocalized (in the calculation this was shared between all the O atoms of the WO_3 host lattice), can be ruled out because of wide disagreement with the observed I_{400}/I_{100} values. In model 2, where the excess charge is shared by the 12 O atoms surrounding the occupied K^+ sites, and in model 3, in which K and O neutral atoms have been taken, a possible agreement is obtained. Calculations for K^+ ions with excess negative charge in the vacancy planes give even worse agreement with experiment than model 1. In other words observations agree approximately with any model in which a neutral charge balance is maintained within the immediate volume of the tunnel sites. Since observations on diffuse electron scattering appear to rule out the formation of K–O–K bonding, and since oxidation from the (presumably ionic) bronze occurs continuously over an O composition without disturbing

Table 2. *Structure factors calculated for the vacancy-ordered structure,* $K_xWO_{(3+y)}$, *for the* $h00$ *reflexions with* $h=1$ *to* 8

(*a*) Both electron and X-ray structure factors (ELECT SF and X-RAY SF) for (i) the oxidized structure with $y=x/2$, and (ii) the structure with $y=0$, assuming K^+ ions in both cases.

h	(i) ELECT SF	(i) X-RAY SF	(ii) ELECT SF	(ii) X-RAY SF
1	0·288	20·98	0·339	16·52
2	−0·456	−20·83	−0·623	−16·41
3	0·482	20·54	0·612	16·22
4	−1·495	−246·8	−1·278	−259·3
5	0·412	19·70	0·468	15·65
6	−0·369	−19·17	−0·392	−15·28
7	0·332	18·57	0·328	14·87
8	6·475	797·9	6·456	786·8

(*b*) Electron structure factors calculated for different ionicity models all with $y=x/2$. (i) K^+,O^- ions in the tunnels with the balance of negative charge shared by O atoms neighbouring K^+ sites. (ii) The K^+O^- tunnel occupation, with the balance of negative charge distributed uniformly throughout the lattice. (iii) K + O neutral atoms in the tunnel sites.

h	(i) ELECT SF	(ii) ELECT SF	(iii) ELECT SF
1	0·288	2·712	0·547
2	−0·456	0·865	−0·522
3	0·482	0·549	0·485
4	−1·495	−1·495	−1·57
5	0·412	0·370	0·400
6	−0·369	−0·332	−0·361
7	0·331	0·306	0·327
8	6·475	6·475	6·469

Table 3. *Comparison of observed and calculated structure-factor ratios for* $K_xWO_{(3+y)}$

(*a*) The F_{800}/F_{700} ratio for X-ray diffraction as a function of composition

Observed	F_{800}/F_{700} (calculated)	
	$y=x/2$, $x=0·27$	$y=0$, $x=0·27$
37 ± 2	43	53

(*b*) The I_{400}/I_{100} ratio for electron diffraction as a function of ionicity. The calculated values are, in the first row, kinematic (F^2_{400}/F^2_{100}), and the remainder are obtained by a systematic interaction calculation for the $h00$ reflexions. The structure factors were obtained for three different electronic models (see text).

Observed	Thickness (Å)	I_{400}/I_{100} (calculated) Model 1 K^+ unscreened	Model 2 K^+ screened	Model 3 K neutral
15 ± 3	Kinematic	0·3	27	8
	Dynamic			
	100	0·5	24	11
	150	0·9	19	12
	200	0·7	14	11
	250	0·3	10	8
	300	0·1	7	6

* The measured mean crystal-plate thickness was $\simeq 1\frac{1}{2}$ μm or $\frac{1}{3}$ of the extinction length for the 800 reflexion. However, absorption and curvature considerably reduce effect of the extinction for this specimen.

subcell dimensions appreciably, it is suggested that model 2, with K^+ ions electrostatically bonded to the host lattice, is the most probable. In this model, as oxidation proceeds some of the negative lattice charge is captured by O atoms, which then occupy sites without radically changing the electrostatic environment.

Finally, a brief study was made of the original black, and reduced, tungsten bronze to see if any type of ordering could be detected by electron diffraction, other than the doubling of the *c* axis reported originally by Magnéli & Blomberg (1951). Samples of this material were ground and examined by selected-area diffraction. Most of the crystals examined had the hexagonal structure. The patterns from these showed no measurable diffuse scattering but a twofold superlattice was recorded in upper layer lines from at least some of the crystals. However, no extra reflexions were visible in the zero layer of [001] projection. It is therefore feasible that the twofold *c* axis is the same as reported by Magnéli & Blomberg, and that it is associated with a doubling of the *a* axis; this doubling may be very difficult to detect by X-ray diffraction. The observed superlattice shown in Fig. 7 is different in character from the one described here for the oxidized structure, since the latter has a strong contribution in the *h*00 line.

7. Conclusions

From this study we conclude that: (*a*) superlattice formation occurs in the oxidized tungsten bronze as a result of two almost independent processes; (*b*) oxidation (and reduction) occurs continuously without appreciable dimensional disturbance of the host lattice.

In conclusion, it would be of interest to investigate the reduced bronze more thoroughly, and to examine consequences of the evident mobility of O in the structure.

The author wishes to thank Mr Frank Bailey for continuous cooperation in operating the high-temperature furnaces, and Professor Kihlborg for helpful discussions and criticism. In addition, the cooperation of Monash University Chemistry Department, and Dr Bryan Gatehouse in particular, in providing samples of tungsten bronze made by solid-state reaction, is gratefully acknowledged.

References

BURSILL, L. A. & HYDE, B. G. (1972). *Nature Phys. Sci.* **240**, 122–124.

DENNE, W. A. & GOODMAN, P. (1973). *Acta Cryst.* B**29**, 2314–2315.

DESCHANVRES, G., DESGARDIN, G., RAVEAU, B. & THOMAZEAU, J. C. (1967). *Bull. Soc. Chim. Fr.* **12**, 4537–4541.

GOODMAN, P. & MCLEAN, J. D. (1976). *Acta Cryst.* B**32**, 3285–3286.

MAGNÉLI, A. & BLOMBERG, B. (1951). *Acta Chem. Scand.* **5**, 372–378.

Acta Cryst. (1976). B**32**, 3285

Direct Imaging of Ordering in $K_xWO_{(3+y)}$

BY P. GOODMAN AND J. D. MCLEAN

Division of Chemical Physics, CSIRO, P.O. Box 160, *Clayton, Victoria, Australia* 3168

(*Received* 23 *January* 1976; *accepted* 15 *March* 1976)

Lattice images from vapour-grown crystals of $K_xWO_{(3+y)}$ with $x \simeq 0{\cdot}27$ and $y \simeq x/2$ show that long-range ordering of 26 Å periodicity perpendicular to the (*h*00) planes is consistent with a two-dimensional ordering of vacancies amongst the K^+ ion sites. The independent nucleation of long-range order in neighbouring crystal regions during the process of oxidation is shown in the micrographs.

Crystals of $K_xWO_{(3+y)}$ with $x \simeq 0{\cdot}27$ and $y \simeq x/2$ grown from the vapour phase at above 1300 °C give electron diffraction patterns which exhibit two superstructures, one arising from the W and one from the K lattice (Goodman, 1976). The diffraction evidence shows that the K^+ structure has a planar ordering, but the nature of the ordering cannot be definitely established from diffraction evidence alone. For this purpose high-resolution electron micrographs were taken, from the *h*00 systematic reflexions. The crystals used were taken directly from the vapour-grown preparation. To assist with the interpretation of the transmission micrographs a series of scanning electron micrographs was taken from crystals typical of the specimens used for transmission study. These micrographs showed approximately plane-parallel lamellae, with discontinuous changes in thickness (Fig. 1). Thin regions frequently occurred along the edges, and these regions were typically 200–300 Å thick.

Fig. 2(*a*) shows a typical region near an edge, with